Electronic Supplementary Information

Pyrazolate-based MOFs with open Zn^{2+} sites for highly effective and rapid adsorption of iodine in water

Xin-Dan Zhang,[a,d] Yong-Zheng Zhang,[a,d,*] Tingting Li,[a,e] Yu-Xiang Zuo,[a] Xiao-Nan Li,[a] Da-Shuai Zhang,[a,d] Longlong Geng,[a,d] Bin Wang,[c,*] Hongliang Huang,[b,*] Xiuling Zhang,[a,d,e,*]

[a] *Shandong Provincial Key Laboratory of Monocrystalline Silicon Semiconductor Materials and Technology, Shandong Universities Engineering Research Center of Integrated Circuits Functional Materials and Expanded Applications, College of Chemistry and Chemical Engineering, Dezhou University, Dezhou 253023, P. R. China.*

[b] *State Key Laboratory of Separation Membranes and Membrane Processes, School of Chemical Engineering and Technology, Tiangong University, Tianjin 300387, China*

[c] *State Key Laboratory of Radiation Medicine and Protection, School for Radiological and Interdisciplinary Sciences (RAD-X), and Collaborative Innovation Center of Radiation Medicine of Jiangsu Higher Education Institutions, Soochow University, Suzhou 215123, China*

[d] *School of Chemistry and Chemical Engineering, Shandong University of Technology, Zibo-255000,China*

[e] *School of Environmental and Chemical Engineering, Xi'an Polytechnic University, Xi'an, 710048, PR China*

Section 1. Experimental

Chemicals and reagents

All the reagents and solvents are commercially available and used without further purification. Benzenamine,4-(1H-pyrazol-4-yl)-N, N-bis[4-(1H-pyrazol-4-yl)phenyl]-(H_3TPPA) and Benzoic acid are purchased from Jilin Zhongkeyan Scientific and Technological Co., Ltd.. Zinc nitrate hexahydrate ($Zn(NO_3)_2 \cdot 6H_2O$), N,N-dimethylformamide (DMF，99%), and anhydrous ethanol (EtOH, 99.7%) are provided by Guoyaoji Chemical Reagent Co., Ltd. Iodine (AR) is purchased from Shanghai Titan Scientific Co., Ltd. We specifically used non-radioactive iodine (^{127}I) for the iodine adsorption experiments to ensure the safety of the experimental process and to minimize environmental impact. Potassium iodide (AR) is purchased from Tianjin Fuchen Chemical Reagent Factory. Activated carbon is purchased from Acros NORITU A SUPRA. Acetic acid (99.8%) is purchased from Thermo Fisher Scientific (China) Co., Ltd.

Characterizations

Powder X-ray diffraction data (PXRD) analysis of powders were recorded on a Bruker SMART APEXII CCD diffractometer in reflection mode using Mo-Kα radiation (λ=0.71073 Å. The 2θ range from 5˚ to 50˚ was scanned with a step size of 0.01˚. Fourier transform infrared spectroscopy (FT-IR) analysis was performed on a Shimadzu FTIR-8400S spectrophotometer. Spectra were recorded in the 4000 to 400 cm^{-1} wavenumber range. Thermogravimetric analysis (TGA) data were recorded by using a STA449FF5 thermogravimetric analyzer with a heating rate of 10 °C min^{-1}

under N_2 atmosphere. The surface areas and pore properties were investigated by N_2 adsorption and desorption at 77 K using BSD-PMC. X-ray photoelectron spectroscopy (XPS) was recorded on a Kratos ASAM800 spectrometer. The powders morphologies were observed via energy-dispersive X-ray spectrometry-scanning electron microscopy (EDS-SEM). Raman spectra were obtained using a Lab Ram HR Evolution Raman microscope with a 785 nm laser and a 1200 lines/mm grating. UV−vis spectra were recorded on a Shimadzu UV1600 spectrometer. The pore-size-distribution curves were obtained from the adsorption branches using the density functional theory (DFT) method.

Crystal Data Collection and Refinement

SCXRD data for two crystal samples were collected using a Bruker diffractometer with the Mo-Kα radiation (λ = 0.71073 Å) at 296 K. Absorption correction was performed using the SADABS program.[S1] The structures were solved by the direct method and refined by full-matrix least-squares on F2 with anisotropic displacement using the SHELXTL software package.[S2] Non-hydrogen atoms on the frameworks were refined with anisotropic displacement parameters during the final cycles. Hydrogen atoms of organic ligands were calculated in the ideal positions with isotropic displacement parameters, except those in the coordinated μ_3-OH/H_2O groups. Although selected hydrogen atoms were not added but were calculated into molecular formula of the crystal data. For all MOFs, the volume fractions of disordered solvents in pores could not be modeled in terms of atomic sites, but were treated by using the MASK routine in the Olex2 software package.[S3] Crystal data can be found in Table S1. More

details can be found in CCDC: DZU-109, 2404967; DZU-110, 2404968

Iodine vapor uptake capacity

Experiments on the adsorption of iodine vapor were determined by gravimetric measurements[S4]. The adsorbents were used as prepared or pre-activated at 348 K for 10 h. Then, 10 mg of adsorbent was weighed in small weighing vials, which were located in a sealed container with iodine pellets kept at the bottom. The container was placed under 348 K for adsorption and the vials containing residual adsorbent were weighed over different time periods.

The amount of adsorbed iodine was determined using the following equation:

$$q_t = \frac{m_t - m_0}{m_0}$$

where q_t (g g^{-1}) is the amount of iodine-adsorbed per gram of adsorbent at time t (min). m_0 (mg) and m_t (mg) are the initial and residual weight of the vials containing the adsorbent, respectively.

Adsorption model

Pseudo-first-order kinetics model:

$$log(q_e - q_t) = logq_e - \frac{k_1 t}{2.303}$$

Pseudo-second-order kinetics model:

$$\frac{t}{q_t} = \frac{1}{k_1 q_e^2} + \frac{t}{q_e}$$

where q_t and q_e (mg g^{-1}) are the adsorption capacity at time t and equilibrium time,

respectively. k_1 (h^{-1}) and k_2 (g mg^{-1} min^{-1}) are the pseudo-first order model rate constant and the pseudo-second order model rate constant, respectively[S5].

The Langmuir isotherm model:

$$\frac{C_e}{q_e} = \frac{C_e}{q_m} + \frac{1}{bq_m}$$

The Freundlich isotherm model:

$$logq_e = logK_F + \frac{1}{n} logC_e$$

where q_e is the equilibrium adsorption capacity (mg g^{-1}), C_e is the equilibrium concentration (mg L^{-1}), and q_m and b are Langmuir constants related to maximum adsorption capacity and binding energy, respectively; K_F and n are empirical constants that indicate the Freundlich constant and heterogeneity factor, respectively[S6].

Iodine adsorption efficiency from aqueous media

The adsorbent (10 mg) was immersed in an aqueous iodine solution prepared by dissolving 20 mg of KI and 10 mg of I_2 in 10 mL of water. Subsequently, the aqueous solution was monitored using UV-Vis spectroscopy and ion chromatography. The iodine removal efficiency of the corresponding adsorbent was calculated using the following equation[S7]:

$$\text{Iodine Removal Efficiency}(\%) = \left(1 - \frac{c_t}{c_0}\right) \times 100\%$$

where C_0 (ppm) and C_t (ppm) are the concentrations of aqueous iodine before and after adsorption, respectively.

Dynamic flow-through adsorption efficiency

A column with a cross-sectional area of 4 mm^2 was packed with 10 milligrams of adsorbent. Then, KI_3 aqueous solution (I_3^-: 10 mg of KI and 5 mg of I_2 dissolved in 100 ml of water, corresponding to 1-30 equivalents of iodine) was passed through the column at a flow rate of 1 mg mL^{-1} for the adsorbent and 1 mg per minute for activated carbon (ACs), in the presence or absence of competing anions (such as Cl^-, Br^-, NO_3^-, or SO_4^{2-}) or under different pH conditions (4-10), with the flow rates precisely controlled by a syringe pump. The eluent was directly analyzed using UV/Vis spectroscopy. The iodine removal efficiency of the adsorbent was calculated using the following equation[S8]:

$$\text{Dynamic flow-through adsorption efficiency} = \left(1 - \frac{c_t}{c_0}\right) \times 100\,\%$$

Section 2. Computational Models and Methods

To investigate the interaction energies between I_3^- ion and the MOFs, the first principles density functional theory calculations were performed using CP2K program [S9]. Core electrons were represented with norm-conserving Goedecker-Teter-Hutter pseudo potentials and the valence electron wavefunction was expanded in a double-zeta basis set with polarization functions along with an auxiliary plane wave basis set with an energy cutoff of 400 eV. The generalized gradient approximation exchange-correlation functional of Perdew, Burke, and Enzerhof (PBE) was used. Each configuration was optimized with the Broyden-Fletcher-Goldfarb-Shanno (BGFS) algorithm with SCF convergence criteria of 1.0×10^{-8} au. To compensate the long-range van der Waals dispersion interaction between the I_3^- ion and the DZU-109 and DZU-

110, the DFT-D3 scheme with an empirical damped potential term was added into the energies obtained from exchange-correlation functional in all-calculations.

Section 3. Additional Figures

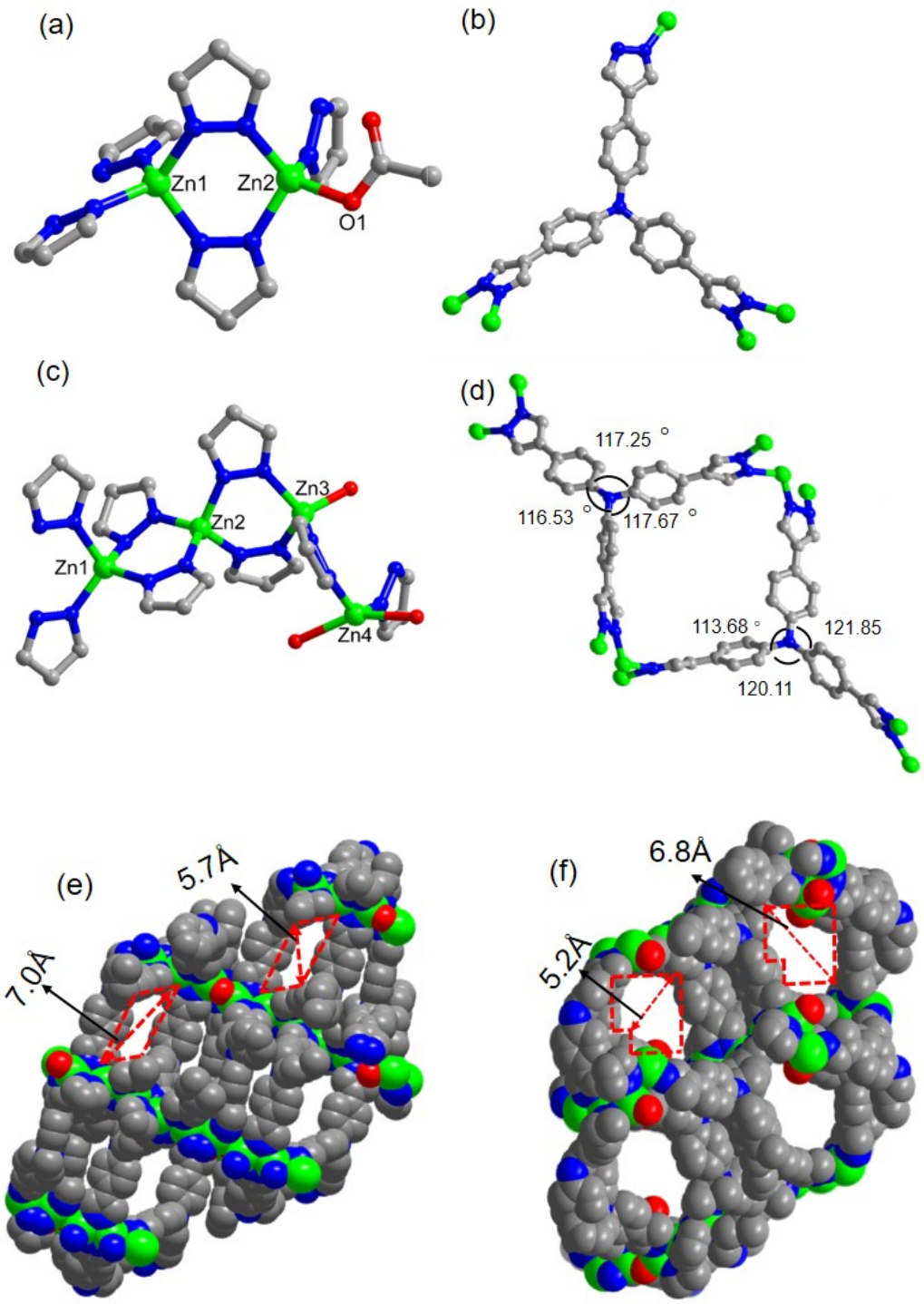

Fig. S1 Zn(II) coordination environment diagram (a) DZU-109 (b) DZU-110, coordination mode diagram of pyrazole group with Zn(II) on $TPPA^{3-}$ ligand (c) DZU-109 (d) DZU-110 and dimensions of DZU-110 in directions (e) 100 and (f) 110.

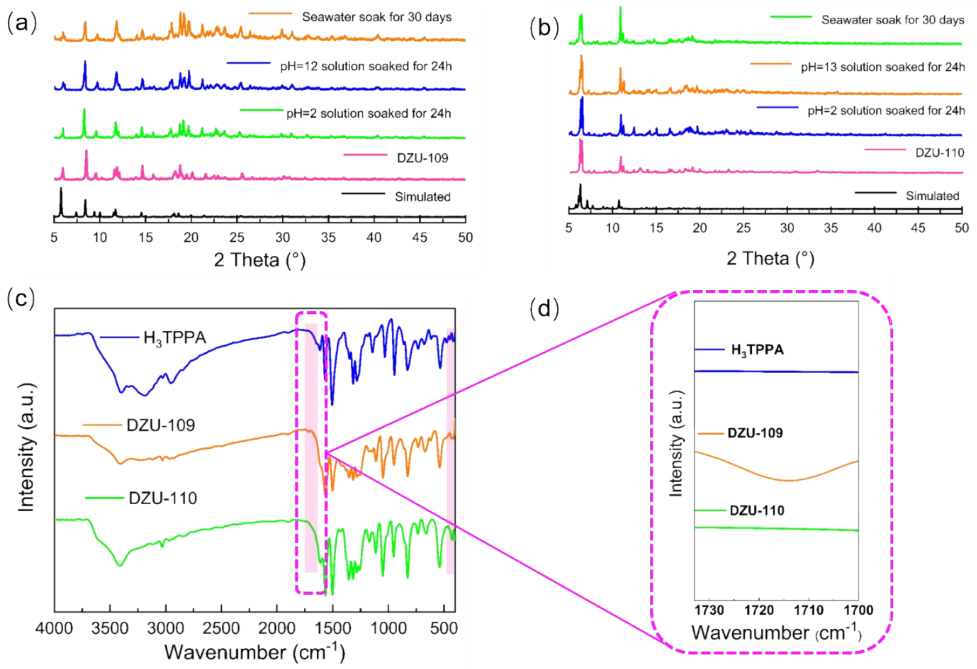

Fig. S2. PXRD patterns of (a) DZU-109, (b) DZU-110 (c) FT-IR pattern of DZU-109 and DZU-110 and (d) enlarge the picture.

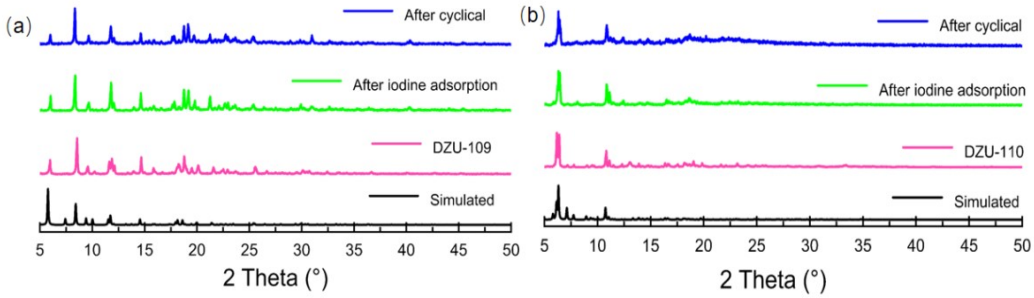

Fig. S3. PXRD patterns after test.

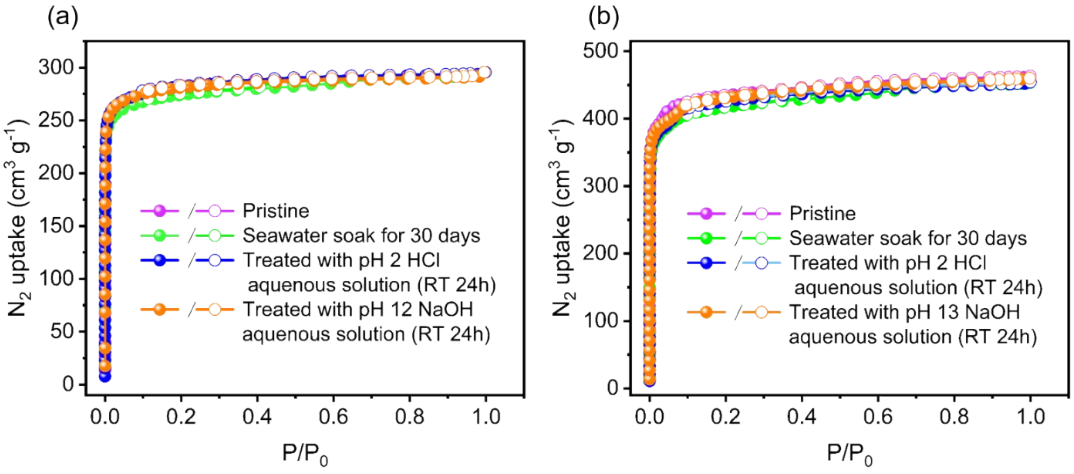

Fig. S4. 77 K N_2 adsorption isotherms of (a) DZU-109 and (b) DZU-110 and their samples under different treatment conditions.

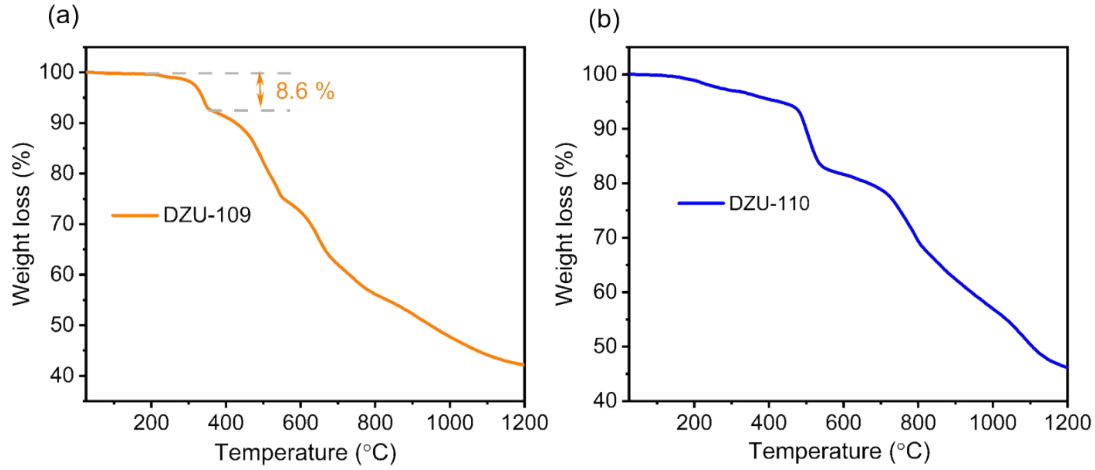

Fig. S5. TGA curves of (a) DZU-109 and (b) DZU-110.

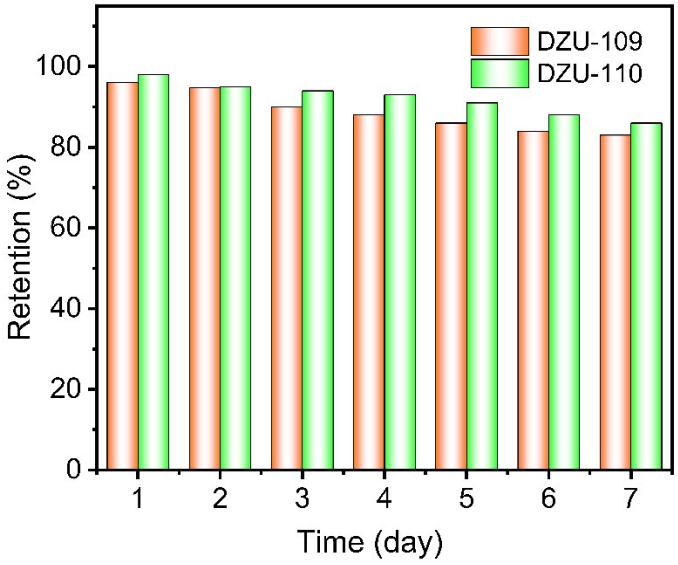

Fig. S6. Time variation of iodine release from I_2@MOF in the environment.

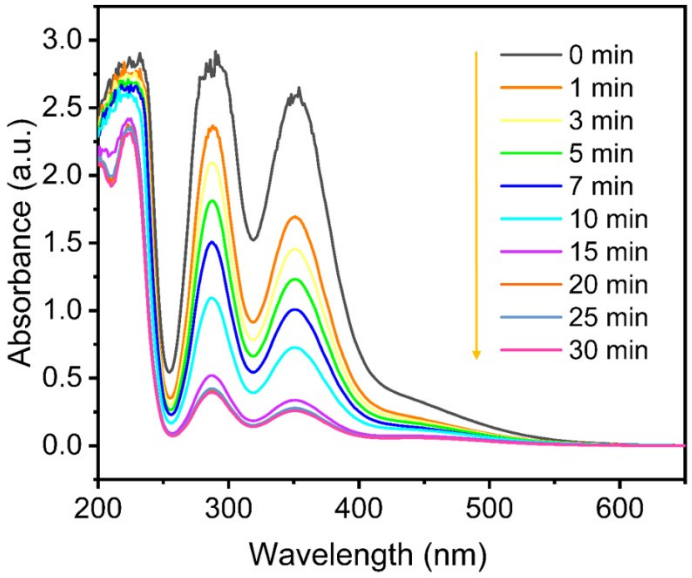

Fig. S7. Time-varying I_3^- absorption UV-VIS spectrum of DZU-109.

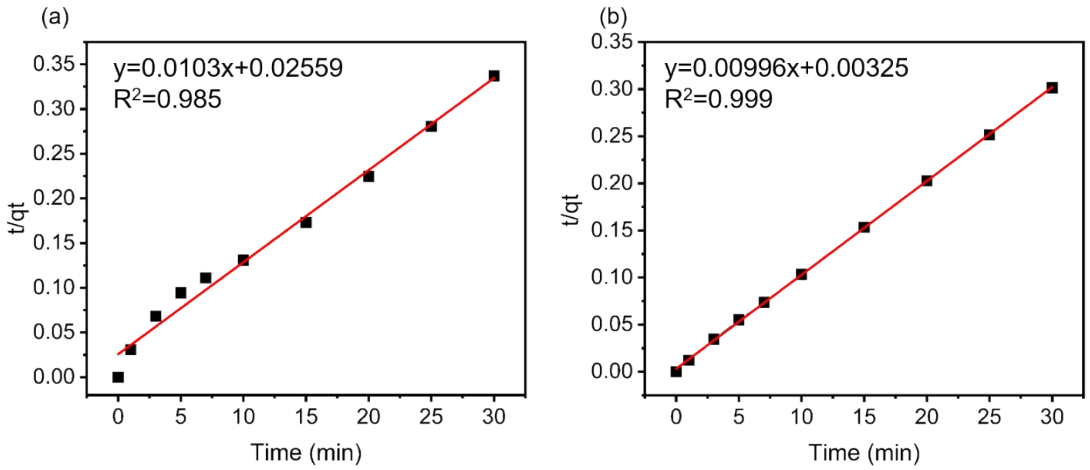

Fig. S8. Adsorption kinetics analysis of aqueous solution (a) DZU-109. (b) DZU-110.

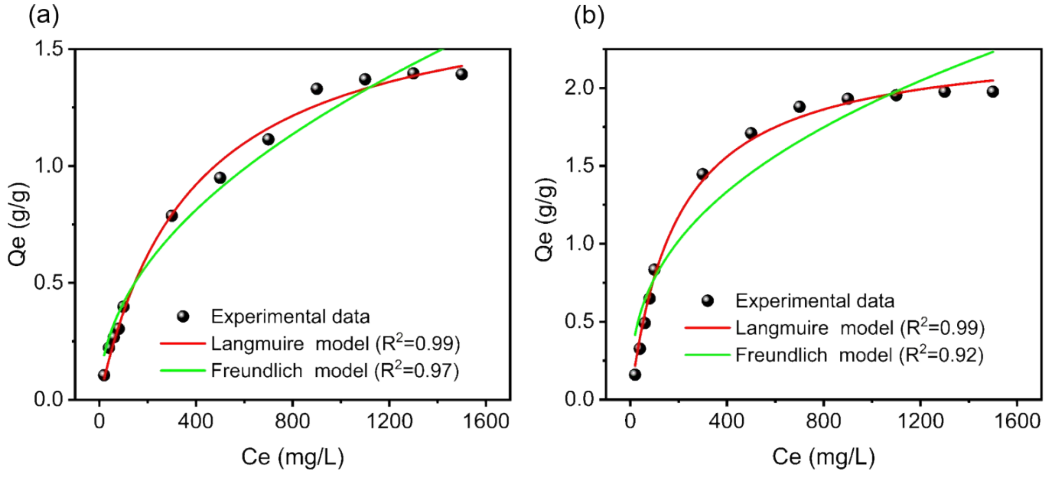

Fig. S9. Adsorption isotherm of (a) DZU-109, (b) DZU-110.

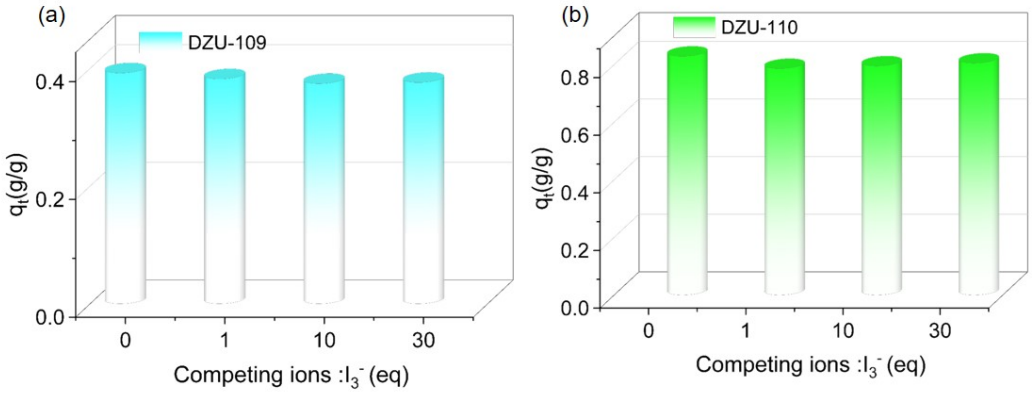

Fig. S10 Iodine uptake from aqueous iodine-containing solutions (100ppm) in the presence of 1–30 equivalents of equal-molar Cl^-, Br^-, NO_3^-, and SO_4^{2-} using DZU-109 and DZU-110.

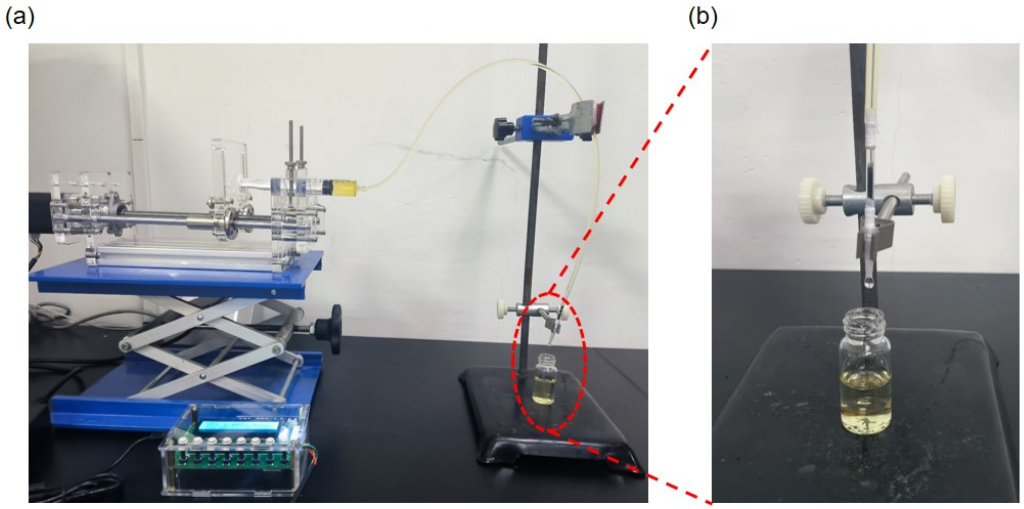

Fig. S11 (a) ACs is used for a flow-through aqueous iodine adsorption experiment with a flow rate of 1.0 mL min^{-1}. (b) Locally enlarged image of ACs.

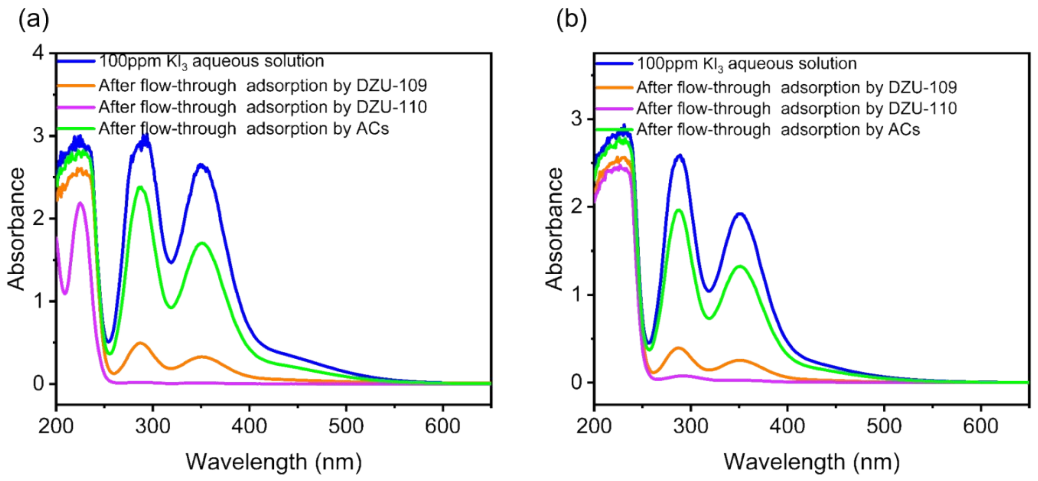

Fig. S12. UV/Vis spectra at pH=4 and pH=10 showed the changes of 100ppm iodine solution before and after MOF and activated carbon (ACs) flow adsorption.

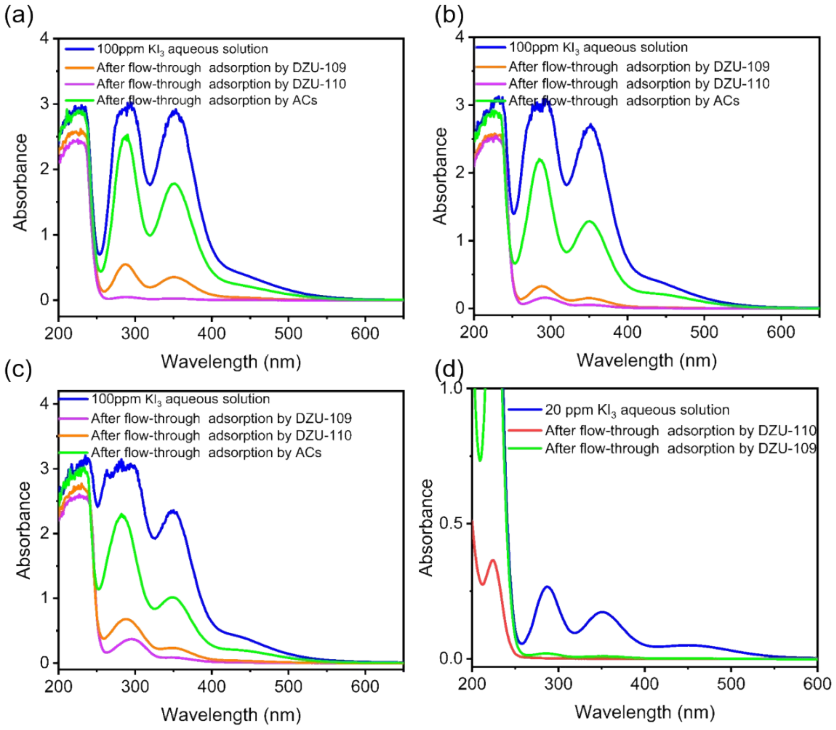

Fig. S13 UV/Vis spectra before and after flow adsorption of iodine solution (100 ppm) by DZU-109 and DZU-110 in the presence of (a) 1, (b) 10 and (c) 30 equimolar Cl^-, Br^-, NO_3^- and SO_4^{2-}, (d) iodine solution (20 ppm).

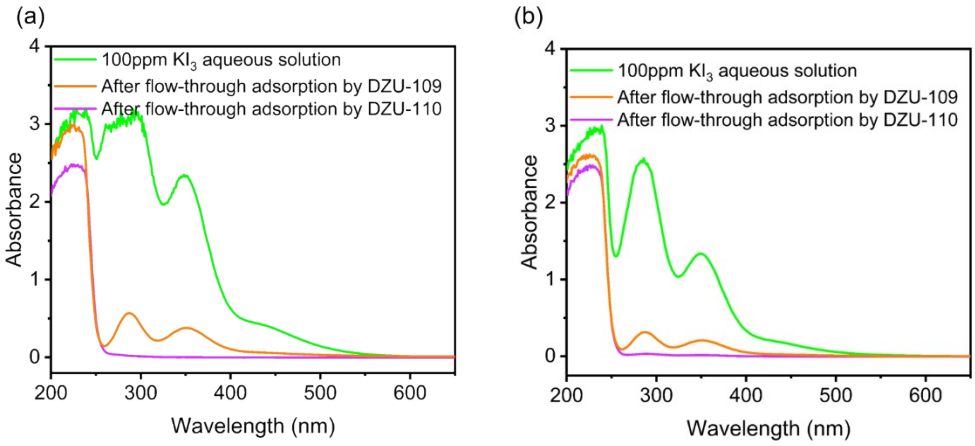

Fig. S14. UV/Vis spectra before and after flow adsorption of iodine solution (100 ppm) by DZU-109 and DZU-110 in the presence of (a) pH=4 and 30 times equimolar Cl^-, Br^-, NO_3^- and SO_4^{2-}, (b) pH=10 and 30 times equimolar Cl^-, Br^-, NO_3^- and SO_4^{2-}.

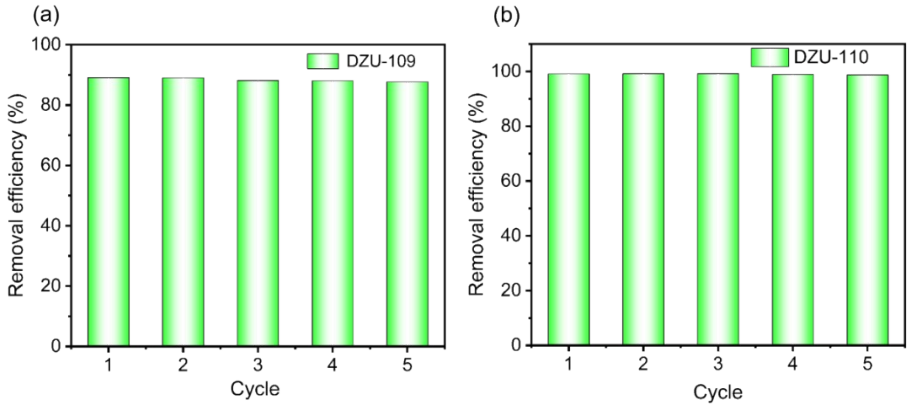

Fig. S15. Five cycles of experiment (a) DZU-109 (b) DZU-110.

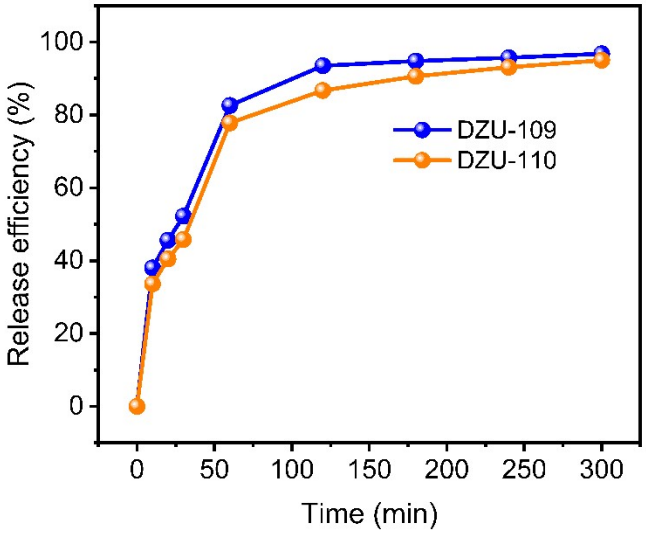

Fig. S16. Release efficiency of I_3^-.

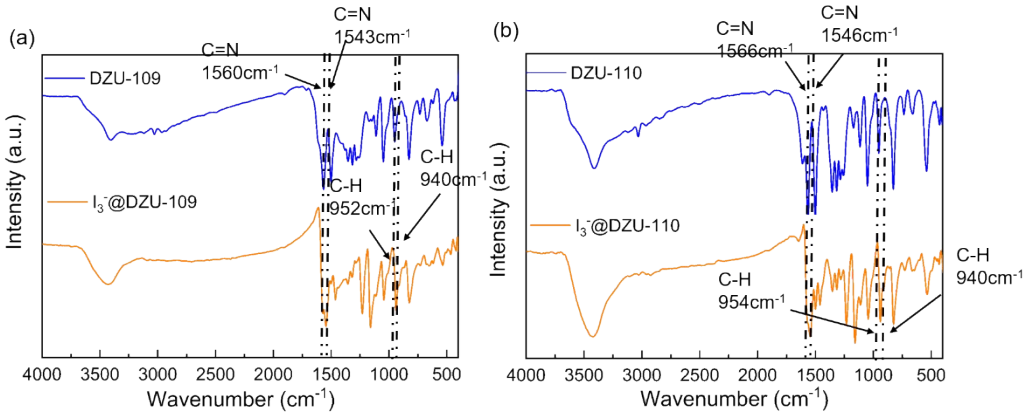

Fig. S17. FT-IR spectrum after iodine adsorption (a) DZU-109 (b) DZU-110.

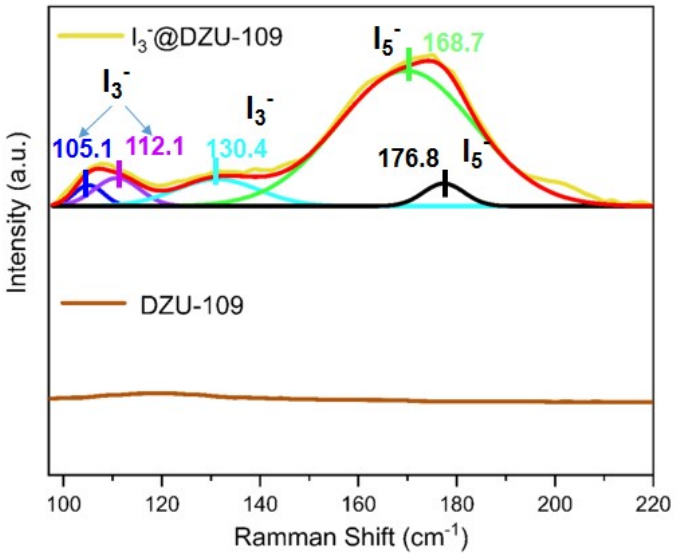

Fig. S18. Raman spectra of DZU-109 after the adsorption of I_3^-.

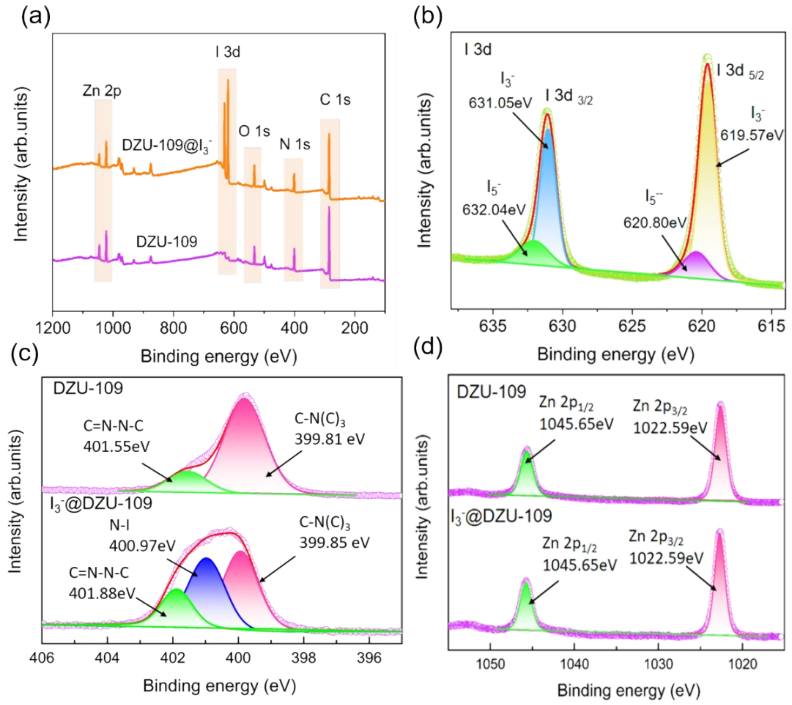

Fig. S19. XPS spectra of DZU-109 before and after the adsorption of I_3^-: (a) XPS Survey, (b) I 3d , (c) N 1s, and (d) Zn 2p.

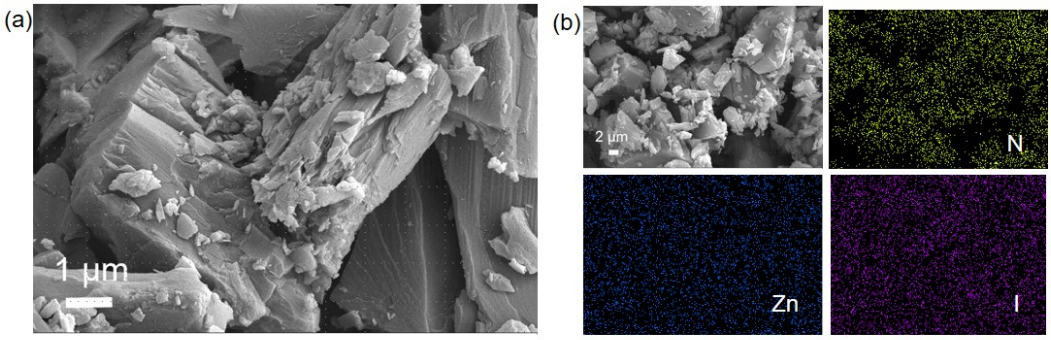

Fig. S20. SEM image and EDS mapping of I_3^- adsorbed DZU-109

Section 4. Additional Tables

Table S1 Crystal data and structure refinements of DZU-109 and DZU-110.

	DZU-109	DZU-110
Empirical formula	$C_{58}H_{44}N_{14}O_4Zn_3$	$C_{108}H_{76}N_{28}O_3Zn_7$
Formula weight	1197.18	2271.52
Temperature/K	296	296
Radiation	MoKα	MoKα
Crystal system	monoclinic	monoclinic
Space group	C2/c	C2/c
a (Å)	24.952(5)	37.767(3)
b (Å)	30.648(6)	15.9977(13)
c (Å)	11.314(2)	32.703(3)
α (°)	90.000	90
β (°)	107.520(4)	111.374(5)
γ (°)	90.000	90
V (Å^3)	8251.(3)	18400(3)
Z	4	4
Dc (g cm^{-3})	0.964	0.817
F (000)	2448.0	4584.0
2θ range for data collection (°)	2.658 to 55.03	4.118 to 54.994
Goodness-of-fit on F^2	0.927	0.981
Final R indexes [I> = 2σ (I)]	R_1= 0.0506, wR_2= 0.1027	R_1= 0.0674, wR_2= 0.2037
Final R indexes [all data]	R_1= 0.1154, wR_2=0.1200	R_1= 0.1127, wR_2= 0.2305
Largest difference in peak and hole (e Å^{-3})	0.29/-0.33	0.70/-1.09

Table S2 Kinetics parameters for Iodine solution capture by DZU-109 and DZU-110.

Type of Kinetics	Parameter	DZU-109	DZU-110
Pseudo-second-order	K_2 (g mg^{-1} min^{-1})	0.42×10^{-2}	3.08×10^{-2}
	R^2	0.985	0.999

Table S3 Summary of the Langmuir and Freundlich isotherm fitting parameters.

MOFs	Langmuir isotherm			Freundlich isotherm		
	q_{max} (g/g)	b (L/mg)	R^2	K_F	n	R^2
DZU-109	1.79	0.00266	0.99	0.04463	2.065	0.97
DZU-110	2.31	0.00518	0.99	0.12976	2.5708	0.92

Table S4 Summary of the reported results for the capture of iodine.

Materials	Q_e (g/g)	K_2(g $mg^{-1}min^{-1}$)	type	reference
DZU-110	2.31	3.08×10^{-2}	MOF	This work
DZU-109	1.79	0.42×10^{-2}	MOF	This work
NH_2-MOF	0.94	0.3×10^{-2}	MOF	[S9]
Zn(ttr)(oAC)	0.8641	0.02×10^{-2}	MOF	48
Zn(tr)(oAC)	0.7145	0.03×10^{-2}	MOF	48
Lac-zn	0.03172	0.002×10^{-2}	MOF	[S10]
N-MOF-PAN	3.61	0.0033×10^{-2}	MOF membrane	53
PCN-223	1.616	/	MOF	37
PCN-233-HPP	1.677	/	MOF	37
3D-MOF1	1.1	/	MOF	56
MIL-125-NH_2@chitosan	0.399	/	MOF composites	[S11]
COF@NH_2-MOF	2.157	1×10^{-2}	COF	[S9]
Amorphous Nanocage $Zn_{12}L_4$	1.731	0.43×10^{-2}	Metallo Organic Cage	[S12]
Crystalline Nanocage $Zn_{12}L_4$	1.487	2.08×10^{-2}	Metallo Organic Cage	[S12]
C-poly-1_5	3.2	0.084×10^{-2}	COF	[S13]
C-poly-1_{20}	4.31	0.062×10^{-2}	COF	[S13]
C-poly-1_{50}	3.97	0.039×10^{-2}	COF	[S13]
C-poly-1_{80}	3.75	0.035×10^{-2}	COF	[S13]
C-poly-1_{100}	3.59	0.034×10^{-2}	COF	[S13]

Section 5. References

[S1] Oxford Diffraction, CrysAlis Pro software. 2010, Ver. 1.171.34, Yarnton, Oxfordshire. Oxford Diffraction Ltd.

[S2] G. M. Sheldrick, A short history of SHELX, Acta crystallographica. Section A, Foundations of crystallography, 2008, 64, 112–122.

[S3] B. Rees, L. Jenner and M. Yusupov, Bulk-solvent correction in large macromolecular structures, Acta Cryst. D, 2005, 61, 1299–1301

[S4] Y. Xie, T. Pan, Q. Lei, C. Chen, X. Dong, Y. Yuan, W. A. Maksoud, L. Zhao, L. Cavallo, I. Pinnau and Y. Han, Efficient and simultaneous capture of iodine and methyl iodide achieved by a covalent organic framework, Nature Communications, 2022, 13, 2878.

[S5] L. Liu, L. Chen, K. Thummavichai, Z. Ye, Y. Wang, T. Fujita and X. Wang, Amino-functionalized MOF-on-MOF architectural nanocomplexes composed for radioactive-iodine efficient adsorption, Chem. Eng. J., 2023, 474, 145858.

[S6] M. Alsalbokh, N. Fakeri, S. Lawson, A. A. Rownaghi and F. Rezaei, Adsorption of iodine from aqueous solutions by aminosilane-grafted mesoporous alumina, Chem. Eng. J., 2021, 415, 128968.

[S7] K. M. A. Qasem, S. Khan, M. N. Ahamad, H. A. M. Saleh, M. Ahmad and M. Shahid, Radioactive iodine capture by metal organic frameworks in liquid and vapour phases: An experimental, kinetic and mechanistic study, Journal of J. Environ. Chem. Eng., 2021, 9, 106720.

[S8] Y. Tang, H. Huang, J. Li, W. Xue and C. Zhong, IL-induced formation of dynamic complex iodide anions in IL@MOF composites for efficient iodine capture, J. Mater. Chem. A, 2019, 7, 18324–18329.

[S9] J. VandeVondele, M. Krack, F. Mohamed, M. Parrinello, T. Chassaing, J. Hutter, Comput. Phys. Commun. 2005, 167, 103-128.

[S10] L. Xu, Q. Zheng, Y. Wang, L. Jiang, J. Jiang and J. Qiu, A pillared double-wall metal-organic framework adsorption membrane for the efficient removal of iodine from solution, Sep. Purif. Technol., 2021, 274, 118436.

[S11] M. El-Shahat, A. E. Abdelhamid and R. M. Abdelhameed, Capture of iodide from wastewater by effective adsorptive membrane synthesized from MIL-125-NH_2 and cross-linked chitosan, Carbohydr. Polym., 2020, 231, 115742.

[S12] J. Wang, M. Chen, H. Zhao, Q. Dong, M. Wang, Z. Wu, W. Zhong, X. Li, D. Liu, T.-Z. Xie, Y. Li, P. Wang and Z. Jiang, Crystalline Metallo–Organic Cage by Triphenylene-Cored Hexaterpyridine for Fast Iodine Capture, Langmuir, 2023, 39, 7337–7344.

[S13] X.-H. Xu, Y.-X. Li, L. Zhou, N. Liu and Z.-Q. Wu, Precise fabrication of porous polymer frameworks using rigid polyisocyanides as building blocks: from structural regulation to efficient iodine capture, Chem. Sci., 2022, 13, 1111–1118.